Effect of Nonstructural Masses on Civil Structures by CUF-Based Finite Element Models

Effect of non-structural masses on civil structures by CUF-based finite element models

A. Pagani*, M. Filippi, M. Petrolo, G. Colonna, E. Carrera

Department of Mechanical and Aerospace Engineering, Politecnico di Torino,
Corso Duca degli Abruzzi 24, 10129 Torino, Italy.

Abstract: *This paper proposes an application of already established higher-order models and, namely, investigates the free vibration analysis of civil engineering structures subjected to non-structural masses. The refined one-dimensional theories adopted are based on the Carrera Unified Formulation (CUF). The stiffness and mass matrices are obtained by means of the principle of virtual displacements in conjunction with the Finite Element Method (FEM). According to CUF, in fact, their formulation is performed in terms of fundamental nuclei, which depend neither on the adopted class of beam theory nor on the FEM approximation along the axis. In order to account for non-structural localized masses, the fundamental nucleus of the mass matrix has been opportunely modified. In this work, Lagrange polynomials have been employed in the framework of CUF to develop pure translational displacement-based refined beam models. The models obtained using this approach are referred, in the literature, to as Component Wise (CW), which allows to model each structural component as a 1D element. The free vibration analysis has been carried out for different cases of non-structural mass distribution in typical civil buildings. The results obtained are compared with classical Solid/Shell FEM solutions from the commercial code MSC Nastran. The capabilities of the CW models are demonstrated, since this formulation is able to replicate the 3D solid results with enhanced performances in terms of computational efforts. Moreover, the importance of taking into account the correct distribution of the non-structural masses is shown to be of fundamental importance in vibration analysis of civil buildings.*

Keywords: Carrera unified formulation, Component-wise, Finite elements, Non-structural mass, Vibration of civil structures.

1 Introduction

Modern structural calculus and computer aided tools are playing a crucial role in the design of constructions that would likely have seemed unimaginable only a few decades ago. In civil engineering, for example, long span bridges and skyscrapers of modern times have seen an extremely rapid evolution. Over the last years the improvement of computational methods such as FEM has remarkably contributed to expand the knowledge in structure engineering. One of the most powerful tools to predict the behaviour of civil buildings is free

*Contact author, e-mail: alfonso.pagani@polito.it

vibration analysis. In fact, in case of severe wind conditions and earthquakes, the response of a building is influenced by its free dynamic behaviour. In order to obtain an accurate prediction, several studies have been devoted to this task over the past and recent years. A ring and a shell finite element for the analysis of the free vibration of cooling towers was described in [1]. The two elements were used to analyze a hyperboloid and a tower similar to those at Didcot Power Station. The free vibration analysis of column supported cooling towers was also investigated in [2]. A finite-element model for the investigation of the dynamic characteristics of the Kap Shui Mun Bridge in Hong Kong was developed in [3], whereas Ren et al. [4] adopted a 3D finite-element model to represent the Roebling Suspension Bridge. Lee et al. [5] derived the governing equations for wall-framed structures from the continuum approach, modeling the whole structure as a shear-flexural cantilever beam with rotational springs. Moreover, Kuang et al.[6] performed free vibration analysis of asymmetric-plan frame structures, focusing on lateral torsional vibration. In [7], the 3D free vibration properties of the cable-stayed Nanjing Bridge on the Yangtze river were analyzed by means of space bar FEM model. Bayrakhtar et al. [8] carried out numerical damage assessments and modal analyses for the *Haghia Sophia* tower through non linear 3D finite element modeling. Riva et al. [9] performed seismic analyses of the *Asinelli* tower adopting a 1D stick model, whereas ring element models were used to obtain the solution properties for free vibration and for transient dynamic problems of a 1000 m solar chimney in [10]. Moreover, Xu et al. [11] adopted a simplified finite element model to design a pair of active mass driver (AMD) systems in order to suppress the wind-induced vibrations of the Canton Tower, whereas the free dynamic behaviour of a masonry bell tower was investigated by means of 3D FEM modeling in [12]. Although the improvements in computational techniques and computer performances allow us to deal with several engineering problems using the 3D FEM models, this approach has proven burdensome as the complexity of the problem increases. To avoid this drawback, simplified models have been used over the years. For example, classical beam models have wide applications for truss and stick simplified elements, whereas the combination of 1D and 2D elements is used for more complex structures, which require plate/shell capabilities. On the other hand, fictitious links are needed to connect beam and plate/shell elements, thus potential inconsistencies are introduced in the geometry of the model. Several refined beam theories have been developed to maintain the simplicity of the 1D model, combined with enriched kinematic field and extended analysis capabilities.

The refined beam theories used in the present work have been developed in the framework of the Carrera Unified Formulation. Initially developed for plates and shell analysis [13, 14], the CUF has been extended to beam structures [15, 16] over the last years. The CUF has the unique feature of a hierarchical formulation, which enables the arbitrary choice of the expansion functions over the cross-section up to the desired order. Moreover, the Component-Wise (CW) approach adopted in [17, 18] allows to model each element of a multi-component structure as a refined beam element. Thus, no inconsistencies are introduced in the model. Free vibration and static analysis of partial and complete civil structures with localized boundary conditions has been carried out in [19] and [20]. Moreover, the influence of non-structural mass on free vibration behaviour

has been evaluated in [21, 22] and in [23] in the case of aerospace structures.

In this paper, the effect of non-structural masses on the free vibration of typical civil engineering structures is investigated. Several engineering problems are deeply influenced by the presence of non non-structural masses. In anti-seismic design, the isolation of acceleration-sensitive equipment from the motion of the supporting structure represents an effective protection from earthquake damage. For this reason, a passive equipment isolation system was designed in [24]. Tests were performed on a scaled experimental model, consisting of a two-storey steel frame and a heavy block-type mass isolated from the second floor. Moreover, in [25], the seismic response of lightweight acceleration-sensitive non-structural components (NSC) mounted on irregular reinforced concrete primary structures was investigated. The analysis was performed by means of non-linear dynamic finite elements. Regular buildings with rigid diaphragms were considered in [26] for analytical investigation in the case of earthquake-induced floor horizontal accelerations. Such accelerations have been responsible for inertia forces causing damage to services and are a major reason for structural damage and even building collapse. Furthermore, the contribution of the NSC to the total stiffness was estimated in [27] for three common forms of tall buildings.

In this work, a C-shaped beam with different boundary conditions has been considered for preliminary assessment. Subsequently, the effects of non-structural masses on the free vibration of an industrial hangar and a three-floor building has been investigated. The results have been compared with those obtained from commercial FEM code analyses. In detail, the Classical Beam Theories (CBT) are presented in Section 2 , whereas Section 3 gives an overview of the higher-order beam theories developed in the framework of CUF. Moreover, Section 4 gives a brief outline of the FEM approach, whereas in Section 5 the results obtained using the proposed CW approach are presented. Section 6 is devoted to the conclusions.

2 Classical beam theories

Figure 1 shows the Cartesian coordinate system adopted for a generic beam structure. The cross section Ω is normal to the beam axis y, which has boundaries $0 \leq y \leq L$. Although the cross-section reported is rectangular, the validity of the proposed formulation is not affected by this choice. According to the

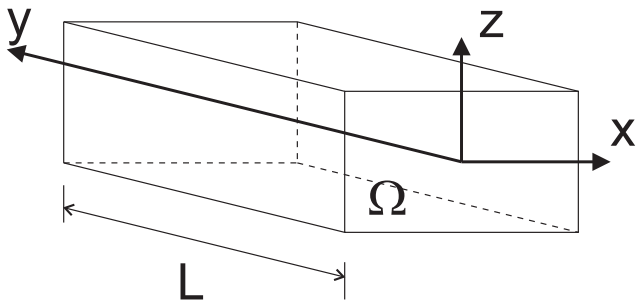

Figure 1: Coordinate frame of the beam.

Euler-Bernoulli Beam Model (EBBM), the kinematic field is

$$\begin{aligned} u_x(x,y,z) &= u_{x1}(y) \\ u_y(x,y,z) &= u_{y1}(y) - x\,\frac{\partial u_{x1}(y)}{\partial y} + z\,\frac{\partial u_{z1}(y)}{\partial y} \\ u_z(x,y,z) &= u_{z1}(y) \end{aligned} \tag{1}$$

where u_x, u_y and u_z are the displacement components of a point along x, y and z axes, respectively; u_{x1}, u_{y1} and u_{z1} are the displacements of the beam axis whereas $-\frac{\partial u_{x1}}{\partial y}$ and $\frac{\partial u_{z1}}{\partial y}$ are the rotations of the cross-section about the z-axis (i.e. ϕ_z) and x-axis (i.e. ϕ_x). Since in EBBM the cross-sectional shear deformation phenomena are neglected, the deformed cross-section is assumed plane and orthogonal to the beam axis. However, several problems (e.g., short beams and composite structures) require the inclusion of shear stresses since their neglect can lead to incorrect results. It is therefore necessary to generalize Eq. (1) and overcome assumption of the orthogonality of the cross-section stated in Euler Bernoulli Beam Theory. The Timoshenko Beam Model (TBM) provides an enhanced displacement field

$$\begin{aligned} u_x(x,y,z) &= u_{x1}(y) \\ u_y(x,y,z) &= u_{y1}(y) + x\,\phi_z(y) - z\,\phi_x(y) \\ u_z(x,y,z) &= u_{z1}(y) \end{aligned} \tag{2}$$

It is clear that TBM constitutes an improvement over EBBM, because the cross-section does not necessarily remain perpendicular to the beam axis after deformation and the original displacement field is enriched by two degrees of freedom (i.e. the unknown rotations, ϕ_z and ϕ_x). For a comprehensive review about classical and modern 1D modelling technique, the reader is referred to [28].

3 Higher-order, hierarchical models by CUF

Classical beam models provide a reasonably good approximation of slender, solid section, homogeneous structures subject to bending phenomena but, in case of short, thin-walled, open cross-section beam analyses, the required degree of accuracy might not be reached. More sophisticated theories, which adopt richer kinematic fields to obtain more accurate 1D models, are needed. By means of the Carrera Unified Formulation (CUF), refined beam models having an arbitrary number of terms in the kinematic field can be developed. The kinematics of a CUF beam model can be summarized as follows:

$$\mathbf{u}(x,y,z) = F_\tau(x,z)\mathbf{u}_\tau(y), \qquad \tau = 1,2,....,M \tag{3}$$

where $\mathbf{F}_\tau$ indicates the functions of the cross section coordinates x and z, $\mathbf{u}_\tau$ is the generalized displacement vector and M indicates the number of terms in the expansion. Since the Einstein notation has been adopted,

the repeated subscript indicates summation. The basis functions adopted to model the displacement field across the section can be different and expanded to any order, since the choice of F_τ and M is arbitrary. The models known in the literature as TE (Taylor Expansion) [15, 29, 30] are obtained considering the Taylor-like expansion polynomials as F_τ functions. It should be noted that Eqs. (1) and (2) are particular cases of the linear ($N = 1$) TE model, which can be expressed as

$$\begin{aligned} u_x(x,y,z) &= u_{x_1}(y) + x\, u_{x_2}(y) + z\, u_{x_3}(y) \\ u_y(x,y,z) &= u_{y_1}(y) + x\, u_{y_2}(y) + z\, u_{y_3}(y) \\ u_z(x,y,z) &= u_{z_1}(y) + x\, u_{z_2}(y) + z\, u_{z_3}(y) \end{aligned} \tag{4}$$

where the parameters on the right-hand side (u_{x_1}, u_{y_1}, u_{z_1}, u_{x_2}, etc.) represent linear displacements and rotations of the beam axis. More details about TE models and the formulation of classical models as particular cases of TE can be found in [31, 32].

The class of hierarchical CUF models used to perform the following analyses adopts the Lagrange polynomials as F_τ functions, therefore these models are referred to as Lagrange Expansion (LE) models, see for example [33, 17, 19]. In LE models, the unknown variables are only pure displacements. This formulation allows us to adopt a Component-Wise (CW) approach. Lagrange elements are in fact used to model the displacement variables in each structural component, whereas arbitrary geometry can be set adopting the iso-parametric formulation. For example, considering one 9-node element L9, the interpolation functions are reported as follows:

$$\begin{aligned} F_\tau &= \tfrac{1}{4}(r^2 + rr_\tau)(s^2 + ss_\tau) && \tau = 1,3,5,7 \\ F_\tau &= \tfrac{1}{2}s_\tau^2(s^2 - ss_\tau)(1 - r^2) + \tfrac{1}{2}r_\tau^2(r^2 - rr_\tau)(1 - s^2) && \tau = 2,4,6,8 \\ F_\tau &= (1 - r^2)(1 - s^2) && \tau = 9 \end{aligned} \tag{5}$$

The coordinates r and s are assumed to vary between -1 and +1. The displacement field in a L9 element can be written in terms of the displacement variables of the problem:

$$\begin{aligned} u_x(x,y,z) &= F_1(x,z)u_{x1}(y) + F_2(x,z)u_{x2}(y) + \cdots + F_9(x,z)u_{x9}(y) \\ u_y(x,y,z) &= F_1(x,z)u_{y1}(y) + F_2(x,z)u_{y2}(y) + \cdots + F_9(x,z)u_{y9}(y) \\ u_z(x,y,z) &= F_1(x,z)u_{z1}(y) + F_2(x,z)u_{z2}(y) + \cdots + F_9(x,z)u_{z9}(y) \end{aligned} \tag{6}$$

where $u_{x1}, ..., u_{z9}$ are the translational components of the nine points of the L9 element. In classical approaches, each component of multi-component structures is modeled in relation with their geometry and scale. On the other hand, CW allows the representation of every part through a 1D CUF model, leading to the use of the same 1D finite element, i.e. the same stiffness matrix in the FEM framework. Moreover, FE models obtained using the CW approach require only physical boundaries, with no need of artificial lines (e.g. beam axes)

and surfaces (plate/shell reference surfaces). Ultimately, the capabilities of the CW models can be adapted by choosing the degree of accuracy required for each component, i.e. the number of elements to be used to discretize the cross section, and the expansion order of the structural model to be adopted.

4 Finite element formulation

4.1 Preliminaries

The reference system chosen is shown in Fig. 1, the stress σ and the strain ϵ components are defined as follows:

$$\begin{aligned} \boldsymbol{\sigma} &= \{\sigma_{yy}, \sigma_{xx}, \sigma_{zz}, \sigma_{xz}, \sigma_{yz}, \sigma_{xy}\}^T \\ \boldsymbol{\epsilon} &= \{\epsilon_{yy}, \epsilon_{xx}, \epsilon_{zz}\epsilon_{xz}, \epsilon_{yz}, \epsilon_{xy}\}^T \end{aligned} \tag{7}$$

In case of small displacements, the following relation between strains and displacements holds:

$$\boldsymbol{\epsilon} = \boldsymbol{D}\boldsymbol{u} \tag{8}$$

where the linear differential operator $\boldsymbol{D}$ is defined as follows:

$$\boldsymbol{D} = \begin{bmatrix} 0 & \frac{\partial}{\partial y} & 0 \\ \frac{\partial}{\partial x} & 0 & 0 \\ 0 & 0 & \frac{\partial}{\partial z} \\ \frac{\partial}{\partial z} & 0 & \frac{\partial}{\partial x} \\ 0 & \frac{\partial}{\partial z} & \frac{\partial}{\partial y} \\ \frac{\partial}{\partial y} & \frac{\partial}{\partial x} & 0 \end{bmatrix} \tag{9}$$

The stress components can be obtained then by the constitutive law:

$$\boldsymbol{\sigma} = \tilde{\boldsymbol{C}}\boldsymbol{\epsilon} \tag{10}$$

Considering an isotropic material, $\tilde{\boldsymbol{C}}$ can be written as:

$$\tilde{\boldsymbol{C}} = \begin{bmatrix} \lambda + 2G & \lambda & \lambda & 0 & 0 & 0 \\ \lambda & \lambda + 2G & \lambda & 0 & 0 & 0 \\ \lambda & \lambda & \lambda + 2G & 0 & 0 & 0 \\ 0 & 0 & 0 & G & 0 & 0 \\ 0 & 0 & 0 & 0 & G & 0 \\ 0 & 0 & 0 & 0 & 0 & G \end{bmatrix} \tag{11}$$

where G is the shear modulus and λ is the Lamé's parameter. By employing elastic modulus E and Poisson ratio one has

$$G = \frac{E}{2(1+\nu)} \quad \lambda = \frac{\nu E}{(1+\nu)(1-2\nu)} \tag{12}$$

4.2 Fundamental nuclei

Adopting the FEM to discretize the structure along the y axis, the displacement variables are interpolated along the y direction by means of the shape functions N_i:

$$\boldsymbol{u} = F_\tau(x,z)N_i(y)\boldsymbol{q}_{\tau i} \tag{13}$$

Since the classical procedure has been adopted to model the structure along the beam axis, the properties of the shape functions are not reported in the present paper for the sake of brevity. More details on FEM can be found, for example, in [32]. In the present work four-node (B4) 1D elements which lead to a cubic approximation along the y axis have been used. Given the Principle of Virtual Displacement, the internal strain energy L_{int} can be related to the work of the inertial loads L_{ine}:

$$\delta L_{int} = \int_V \delta\boldsymbol{\epsilon}^T \boldsymbol{\sigma}\, dV = -\delta L_{ine} \tag{14}$$

Where δ stands for virtual variation. Considering Eqs. 8, 7 and 13, the virtual variation of the strain energy can be written in a compact form:

$$\delta L_{int} = \delta\boldsymbol{q}_{\tau i}^T \mathbf{K}^{ij\tau s} \boldsymbol{q}_{sj} \tag{15}$$

where $\mathbf{K}^{ij\tau s}$ is the fundamental nucleus of the stiffness matrix and the superscripts indicate the four indexes exploited to expand the elemental matrix: τ and s are related to the expansion functions F_τ and F_s whereas i and j are related to the shape functions N_i and N_j. The fundamental nucleus, which is a 3x3 array, is formally independent of the order of the beam model. The formal expression of the fundamental nucleus, in fact, does not depend on either the expansion order either the choice of F_τ polynomials, therefore any class and order models can be obtained by means of the same fundamental nucleus. Considering the aforementioned properties, the CUF allows to implement with few coding statements any order of multiple class theories. A more detailed explanation of the expansion of nuclei and assembly procedures in FEM framework can be found in [31].

Modal analysis is influenced by inertial loadings acting on the structure. The work of the inertial loadings can be written in terms of virtual variation:

$$\delta L_{ine} = \int_V \rho\ddot{\mathbf{u}}\delta\mathbf{u}^T\, dV \tag{16}$$

In the above equation ρ stands for the density of the material, whereas $\ddot{\mathbf{u}}$ is the acceleration vector. By substituting Eqs. 3 and 13 into Eq. 16 one has

$$\delta L_{ine} = -\delta \boldsymbol{q}_{\tau i}^T \int_l N_i N_j \, dy \int_\Omega \rho F_\tau F_s \, d\Omega \ddot{\mathbf{q}}_{sj} = -\delta \boldsymbol{q}_{\tau i}^T \mathbf{M}^{ij\tau s} \ddot{\mathbf{q}}_{sj} \tag{17}$$

where $\ddot{\mathbf{q}}_{sj}$ indicates the nodal acceleration vector and $\mathbf{M}^{ij\tau s}$ indicates the fundamental nucleus of the elemental mass matrix, whose components are:

$$\begin{gathered} \mathbf{M}_{xx}^{ij\tau s} = \mathbf{M}_{yy}^{ij\tau s} = \mathbf{M}_{zz}^{ij\tau s} = \textstyle\int_l N_i N_j \, dy \int_\Omega \rho F_\tau F_s \, d\Omega \\ \mathbf{M}_{xy}^{ij\tau s} = \mathbf{M}_{xz}^{ij\tau s} = \mathbf{M}_{yx}^{ij\tau s} = \mathbf{M}_{zx}^{ij\tau s} = \mathbf{M}_{yz}^{ij\tau s} = \mathbf{M}_{zy}^{ij\tau s} = 0 \end{gathered} \tag{18}$$

Even in the case of inertial terms, no assumptions have been made on the expansion order of the theory; thus, several refined beam models can be developed using this formulation without any formal change in the fundamental nucleus components.

The algebraic set of equations for the undamped dynamic problems is obtained by substituting the fundamental nuclei into the principle of virtual displacement (Eq. 14) and expanding for CUF fundamental indexes

$$\mathbf{M}\ddot{\mathbf{q}} + \mathbf{K}\mathbf{q} = 0 \tag{19}$$

Considering harmonic solutions, the second-order system of ordinary differential equations above result into a classical eigenvalue problem:

$$(-\omega_k^2 \mathbf{M} + \mathbf{K})\mathbf{q}_k = 0 \tag{20}$$

where $\mathbf{q}_k$ is the *k-th* eigenvector.

4.3 Non-structural mass

Although the contribution of localised non-structural masses in static analysis can be often neglected, their weight may deeply influence the dynamic behaviour of the system. In the framework of the CUF, non-structural masses can be arbitrarily placed into the 3D domain of the beam structure adding the following term to the fundamental nucleus of the mass matrix:

$$\boldsymbol{m}^{i\tau ts} = \mathbf{I} \left[F_\tau \left(x_m, z_m \right) F_s \left(x_m, z_m \right) N_i \left(y_m \right) N_j \left(y_m \right) \right] \tilde{m} \tag{21}$$

where $\mathbf{I}$ is the 3×3 identity matrix and $\tilde{m}$ is the value of the non-structural mass applied at the point (x_m, y_m, z_m).

5 Numerical Results

The following section investigates the influence of non-structural masses on the free vibrations of civil engineering structures. In order to evaluate the reliability of the of the proposed CUF model, MSC Nastran results are reported for comparison.

5.1 C-shaped structure

A C-shaped cross section beam is considered. The structure has the following geometrical features: length $L = 2$ m sides $a = b = 0.2$ m, flanges side-to-thickness ratio $a/t = 10$. The beam is made of steel alloy, having Young's Modulus $E = 198$ GPa , Poisson's Ratio $\nu = 0.3$, density $\rho = 7.85 \times 10^3\ kg\ m^{-3}$. The different FE models shown in Fig. 2 are taken into account for free vibration analysis. In classical and refined FE theories the discretization condensates inertial and stiffness characteristics on the nodes laying on the beam axis, as shown in Fig.2(a). Refined TE models are built by assuming a generic N-order displacement field and by expanding the generalized DOFs above the cross section in the $3D$ space. This allows TE refined theories to overcome the classical theories' limitations, being able to investigate localized effects, warping phenomena and in-plane deformations. In practical applications civil structures are modeled combining $1D$ elements (columns and truss structures), $2D$ elements (walls and floors)(Fig.2(b)) and $3D$ solid elements (e.g. Fig.2(c)) if needed. The combination of kinematically different elements yields to problems of accuracy and fictitious links are often needed. In order to overcome this problem, refined $1D$ theories can be used in the CW approach, modeling the elements of the structure as $1D$ elements. As discussed in [19], each flange is modeled separately (see Fig.2(d)) and then assembled on the cross-sectional plane if a CW approach is adopted. Figure 3 shows the distribution of L-elements above the cross section for the CW analysis.

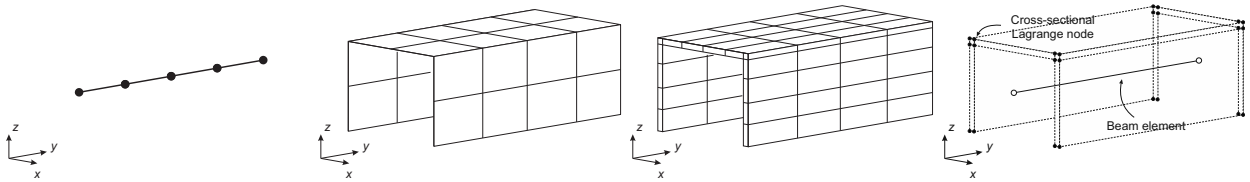

(a) (b) (c) (d)

Figure 2: Different FE models for a C-shaped beam.

First, Clamped-Free (CF) and Clamped-Clamped (CC) boundary conditions are addressed, as shown in Fig. 4a and Fig. 4b, respectively. Table 1 reports the first 5 natural frequencies for different theories. Moreover, in the case of CF boundary conditions, column 1 presents the analytical solution provided by the formula:

$$f_n = \frac{\alpha_n^2}{2\pi}\sqrt{\frac{EI_x}{\rho\Omega L^4}} \quad \alpha_n = 1.875, 4.694, ... \tag{22}$$

where I_x is the moment of inertia with respect to the x axis and Ω indicates the area of the cross section.

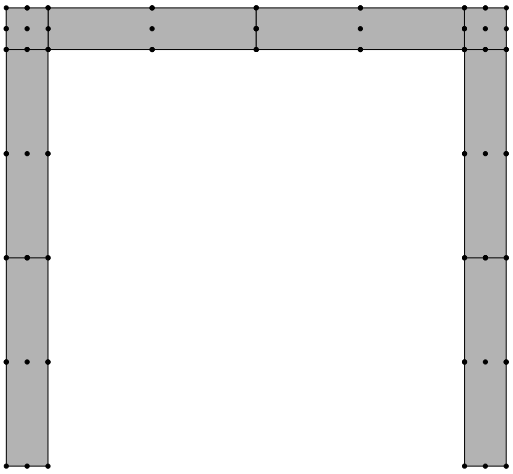

Figure 3: L-elements distribution along the cross section

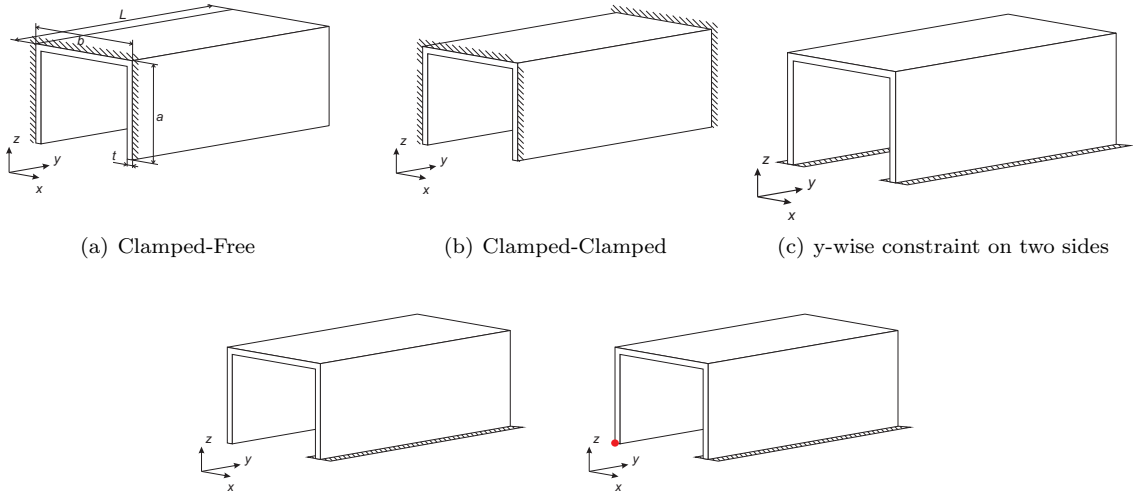

(a) Clamped-Free (b) Clamped-Clamped (c) y-wise constraint on two sides

(d) y-wise constraint on one side (e) Non-structural mass

Figure 4: C-shaped beam boundary conditions and non-structural mass position.

Columns 3 and 4 refer to classical beam theories, EBBM and TBM, whereas the results obtained with refined TE beam models are reported in column 5 and 6, showing respectively frequencies for $N = 2$ and $N = 4$. Results obtained using the CW approach are reported in column 7, whereas results obtained using MSC Nastran models are provided for comparison in columns 8-10. The beam is discretized with 10 $B4$ elements for classical, refined TE and CW models. FE $1D$ Nastran model (NAS1D) consists in 50 2-node CBAR elements, whereas the $2D$ model (NAS2D) is built using 4-node CQUAD4 elements. Moreover, the solid $3D$ model (NAS3D) is obtained using 8-node CHEXA elements. DOFs for each model are reported in row 3. It is clear that classical beam models, NAS1D and lower order TE models provide a good approximation of bending modes when CC and CF boundary conditions are addressed. On the other hand, these tools are ineffective in the detection of global modes involving torsion and coupled torsion/bending phenomena, nor in the description of local modes. In these models, in fact, the cross section of the structure is supposed to be

	Classical and TE models					CW model	MSC Nastran models		
DOFs	Analytical	EBBM (93)	TBM (155)	$N=2$ (558)	$N=4$ (1395)	$8L9$ (4437)	$NAS1D$ (294)	$NAS2D$ (15345)	$NAS3D$ (337305)
Clamped-Free									
Mode 1^c	–	–	–	–	–	32.34	–	31.35	32.01
Mode 2^b	44.67	44.57	44.31	44.61	44.36	44.31	44.25	44.04	44.22
Mode 3^c	–	–	–	–	154.8	105.8	–	105.2	105.4
Mode 4^c	–	–	–	–	241.5	139.8	–	135.9	138.8
Mode 5^b	280.0	275.5	264.9	265.8	260.5	258.0	262.9	255.5	257.2
Clamped-Clamped [19]									
Mode 1^c	-	345.7	323.8	326.4	188.0	124.0	272.3	120.7	123.0
Mode 2^b	-	282.5	266.1	268.3	260.0	256.5	259.2	253.1	255.1
Mode 3^c	-	952.6	802.2	805.7	421.3	286.1	612.4	273.5	208.7
Mode 4^f	-	–	–	–	–	304.8	–	289.3	297.2
Mode 5^f	-	–	–	–	–	348.9	–	331.8	340.8

c: coupled bending mode; b: bending mode on plane yz ; f: flanges mode.

Table 1: Natural frequencies (Hz) of the CF and CC C-shaped beam.

extremely rigid. Although the fourth-order TE model provides acceptable results for global modes, a higher-order TE model is needed to detect local modes, whereas the CW model provides a solution comparable to the NAS3D results, with a dramatic reduction of computational costs. For the second case, the structure is locally constrained, as shown in Fig. 4c and Fig. 4d. Moreover, a non-structural mass equal to the 10 % of the mass of the structure is localized as shown in Fig. 4e. Given the nature of constraints, the classical and refined TE theories cannot be used, unless ad hoc mathematical tools were employed (see [34]). The CW approach, instead, allows us to deal with local constraints, as discussed in [33]. Table 2 reports the first 5 natural frequencies for different boundary conditions and models. Results obtained using the CW approach are reported in column 2 and 3, whereas the results obtained using MSC Nastran models are provided for comparison in column 4 and 5. Moreover, row 3 reports the DOFs for each model.

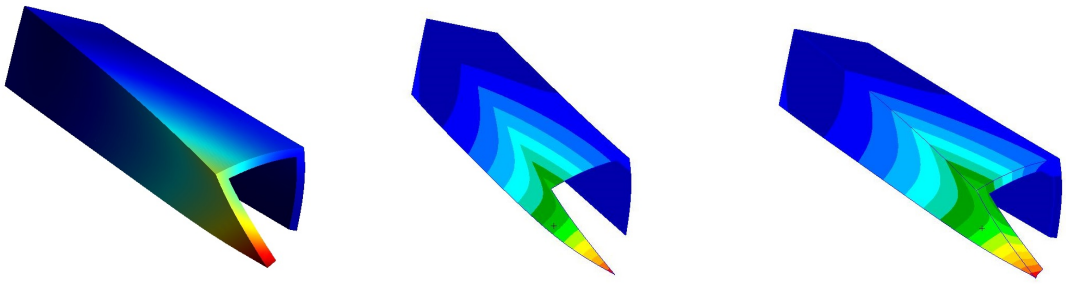

(a) $CW14L9$ (b) $Nastran2D$ (c) $Nastran3D$

Figure 5: 1^{st} modal shape of the y-wise constrained C-shaped beam subject to non-structural mass.

As demonstrated in [19], the refinement of the discretization of the cross section efficaciously improves the solution. The $14L9$ CW model provides a solid-like solution, being capable to detect global and local modes with arbitrary boundary conditions. Moreover, the correspondence with respect to the NAS3D solution is

	CW models		MSC Nastran models	
DOFs	$8L9$ (4185)	$14L9$ (7533)	$NAS2D$ (14645)	$NAS3D$ (334665)
Constraint on both flanges [19]				
Mode 1^b	490.1	455.7	429.3	443.4
Mode 2^b	603.9	574.7	552.2	564.9
Mode 3^b	880.4	855.2	834.9	847.7
Mode 4^b	1250.7	1220.5	1194.3	1212.2
Mode 5^b	1676.9	1625.9	1582.1	1612.3
Constraint on one flange				
Mode 1^s	98.59	97.84	95.82	96.97
Mode 2^s	114.6	113.7	110.7	112.8
Mode 3^s	204.5	198.6	191.1	195.5
Mode 4^s	207.8	201.9	193.9	198.6
Mode 5^s	262.6	258.8	250.3	256.1
Non-structural mass				
Mode 1^s	66.31	65.70	65.00	64.50
Mode 2^s	102.9	101.8	98.75	100.2
Mode 3^s	105.1	103.7	100.8	102.2
Mode 4^s	205.2	199.2	191.7	196.0
Mode 5^s	229.7	224.6	216.1	220.9

b: bending mode on plane xy; s: shell-like mode

Table 2: Natural frequencies (Hz) of the y-wise constrained C-shaped beam.

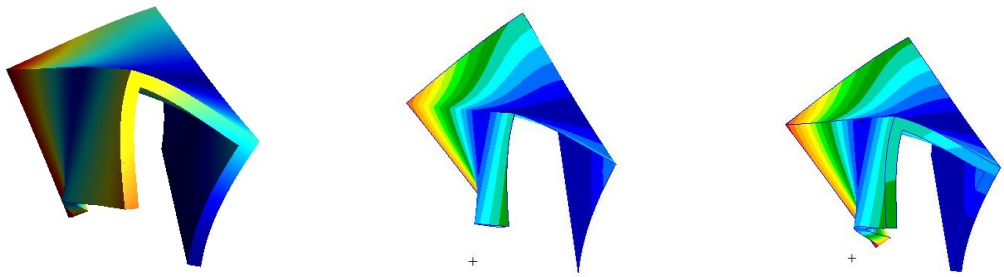

(a) $CW14L9$ (b) $Nastran2D$ (c) $Nastran3D$

Figure 6: 3^{rd} modal shape of the y-wise constrained C-shaped beam subject to non-structural mass.

assessed also when non-structural masses are taken into account. As shown in Fig. 5 and 6, the modal shapes obtained by means of the CW approach are in good accordance with those obtained by means of the Nastran.

5.2 Industrial building

This section considers the industrial building shown in Fig. 7. Results obtained from the free vibration analysis of the initial model, obtained in [19], are reported in Table 3.

In order to investigate the influence of non-structural masses on the natural frequencies of the building, in each case a non-structural mass is applied on the structure, as shown in Fig. 8. In Case A and B the masses applied vary from 1%, 10% and 20% of the mass of the initial structure, consisting in 350×10^3 kg.

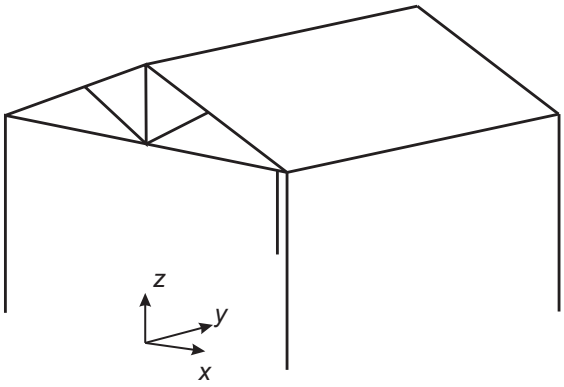

Figure 7: Industrial Building.

In Case C, three combinations of different values of non-structural mass are taken into account: 1% and 5%, 5% and 10%, 10% and 20%. Natural frequencies obtained using CW and MSC Nastran models are given in Table 4 for Case A, Table 5 for Case B and Table 6 for Case C. The difference between the initial model and the one with non-structural mass is evaluated through MAC analysis. Results are shown in Fig. 9, 10, 13, respectively.

DOFs	CW Model (6399)	NAS1D&2D (2836)	NAS3D (143121)
Mode 1^b	0.58	0.49	0.50
Mode 2^t	1.01	0.84	0.87
Mode 3^r	4.41	4.25	4.32
Mode 4^r	11.41	10.68	10.88
Mode 5^r	11.86	11.37	11.53

b: bending mode ; t: torsional mode;
c: coupled roof and truss mode; r: local roof mode.

Table 3: Natural frequencies (Hz) of the industrial building without non-structural mass.

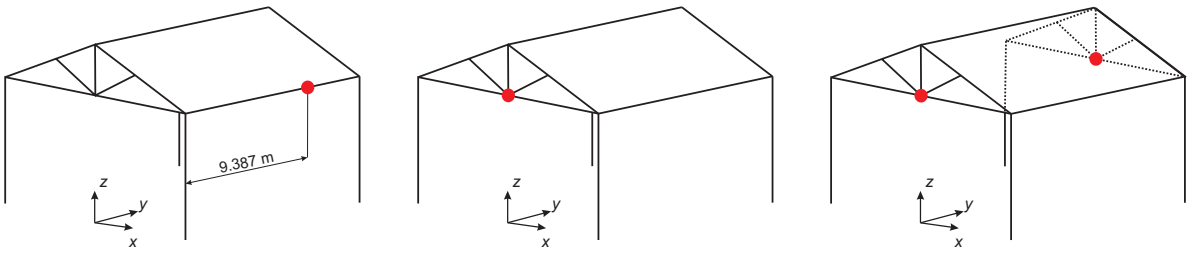

(a) Case A (b) Case B (c) Case C

Figure 8: Three different cases of non-structural masses, industrial building.

It is evident that the proposed formulation is capable to deal with the presence of non-structural masses, the results obtained show good accordance between the LE refined theory and the solution available by means of Nastran commercial code. The CW approach is capable to detect both global modes and roof modes for the

Case A			
DOFs	CW model (6399)	NAS1D&2D (2836)	NAS3D (143121)
Non-structural mass: 1%			
Mode 1^b	0.58	0.49	0.50
Mode 2^t	1.01	0.84	0.86
Mode 3^r	4.30	4.16	4.21
Mode 4^c	9.80	9.23	9.46
Mode 5^r	11.22	10.51	10.71
Non-structural mass: 10%			
Mode 1^b	0.56	0.47	0.48
Mode 2^t	0.95	0.79	0.81
Mode 3^r	3.28	3.21	3.15
Mode 4^c	8.70	8.05	8.14
Mode 5^r	10.47	9.78	10.06
Non-structural mass: 20%			
Mode 1^b	0.53	0.45	0.45
Mode 2^t	0.91	0.76	0.78
Mode 3^r	2.63	2.60	2.51
Mode 4^c	8.30	7.63	7.72
Mode 5^r	10.33	9.65	9.93

b: bending mode; t: torsional mode;
c: coupled roof and truss mode; r: local roof mode.

Table 4: Natural frequencies (Hz) of the industrial building, Case A.

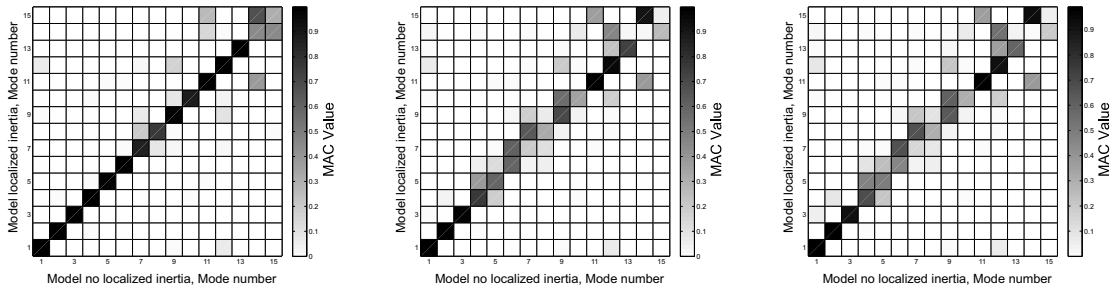

(a) 1% non-structural mass (b) 10% non-structural mass (c) 20% non-structural mass

Figure 9: MAC values between the initial model and the the model with non-structural mass; industrial building Case A, CW approach.

considered problem. From the observation of the MAC matrices reported in Fig. 9, it is clear that the presence of non-structural mass deeply influences the free vibration of the structure. The increase of non-structural mass intensifies the deviation of the results from the initial model.

The comparison between the results obtained using the CW model and those accessible from the commercial code shows that the proposed formulation is capable to deal with the presence of non-structural masses and to evaluate their contribution in the change of local modes. It is clear from Fig. 11 and 12 that these modal shapes involve the roof and the roof truss. Moreover, Fig. 10 highlights the effect of the non-structural mass placed on the roof truss. The modification of the modal shapes with respect to the initial model is

Case B			
DOFs	CW model (6399)	NAS1D&2D (2836)	NAS3D (143121)
Non-structural mass: 1%			
Mode 1^b	0.58	0.47	0.50
Mode 2^t	1.01	0.84	0.86
Mode 3^r	4.41	4.25	4.32
Mode 4^l	–	7.97	8.20
Mode 5^{r+l}	9.82	9.32	9.57
Non-structural mass: 10%			
Mode 1^b	0.56	0.47	0.48
Mode 2^t	0.96	0.80	0.82
Mode 3^l	4.56	3.36	3.29
Mode 4^r	4.40	4.24	4.31
Mode 5^{r+l}	8.95	8.42	8.64
Non-structural mass: 20%			
Mode 1^b	0.53	0.45	0.46
Mode 2^t	0.92	0.77	0.78
Mode 3^l	3.47	2.53	2.47
Mode 4^r	4.39	4.23	4.30
Mode 5^{r+l}	7.94	7.45	7.64

b: bending mode; t: torsional mode.
l: local roof truss mode; r: local roof mode.

Table 5: Natural frequencies (Hz) of the industrial building, Case B.

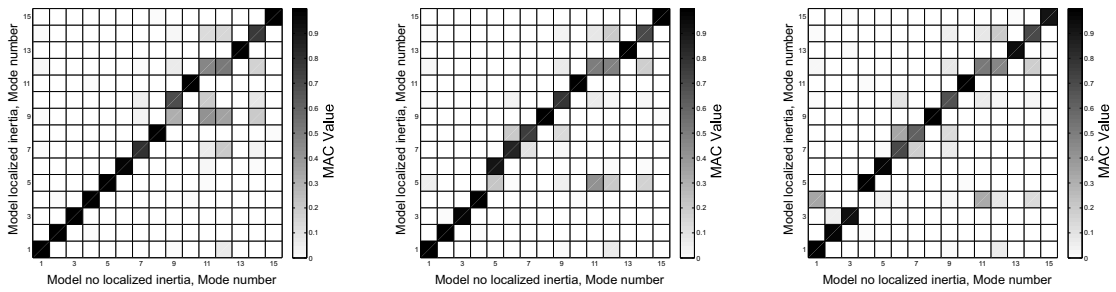

(a) 1% non-structural mass (b) 10% non-structural mass (c) 20% non-structural mass

Figure 10: MAC values between the initial model and the model with non-structural mass; industrial building Case B, CW approach.

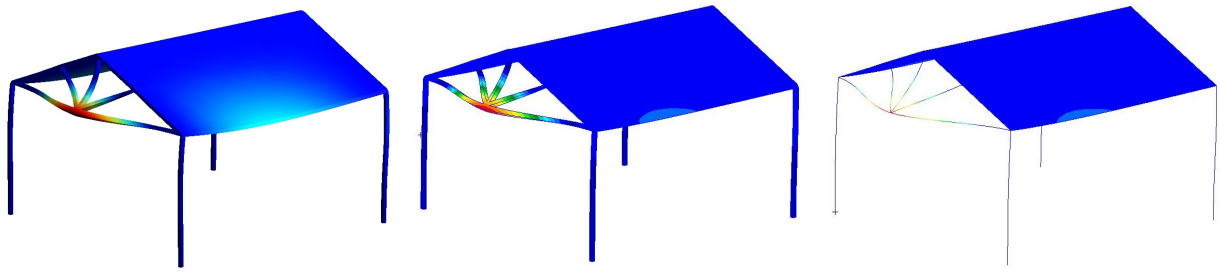

(a) CW Model (b) Solid Model (c) 1D&2D Model

Figure 11: 4^{th} modal shape of the industrial building, 10% non-structural mass, Case B.

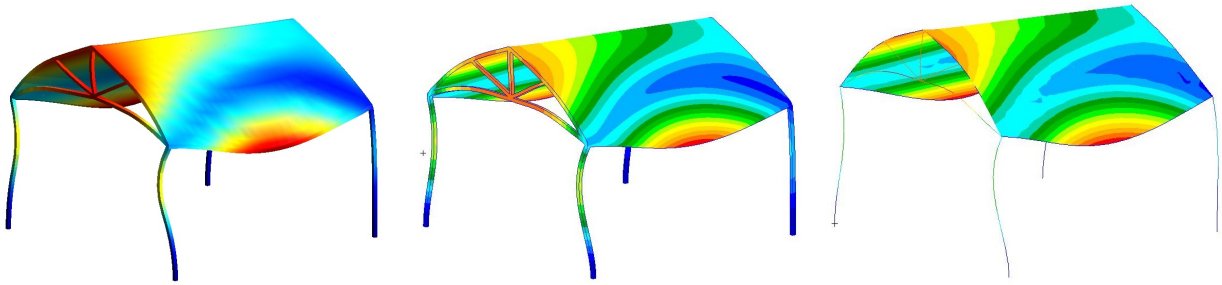

(a) CW Model (b) Solid Model (c) 1D&2D Model

Figure 12: 7^{th} modal shape of the industrial building, 10% non-structural mass, Case B.

blatantly evident in this case.

Case C			
DOFs	CW model (6399)	NAS1D&2D (2836)	NAS3D (143121)
Non-structural mass: 1% and 5%			
Mode 1^b	0.57	0.48	0.49
Mode 2^t	0.97	0.81	0.83
Mode 3^r	4.40	4.24	4.31
Mode 4^l	5.28	4.45	4.40
Mode 5^{r+l}	9.45	8.95	9.19
Non-structural mass: 5% and 10%			
Mode 1^b	0.55	0.46	0.47
Mode 2^t	0.92	0.77	0.78
Mode 3^l	4.55	3.33	3.27
Mode 4^r	4.39	4.23	4.29
Mode 5^{r+l}	8.89	8.34	8.57
Non-structural mass: 10% and 20%			
Mode 1^b	0.51	0.43	0.44
Mode 2^t	0.85	0.71	0.72
Mode 3^l	3.39	2.47	2.42
Mode 4^r	4.37	4.21	4.28
Mode 5^{r+l}	7.92	7.43	7.61

b: bending mode; t: torsional mode.
l: local roof truss mode; r: local roof mode.

Table 6: Natural frequencies (Hz) of the industrial building, two non-structural masses.

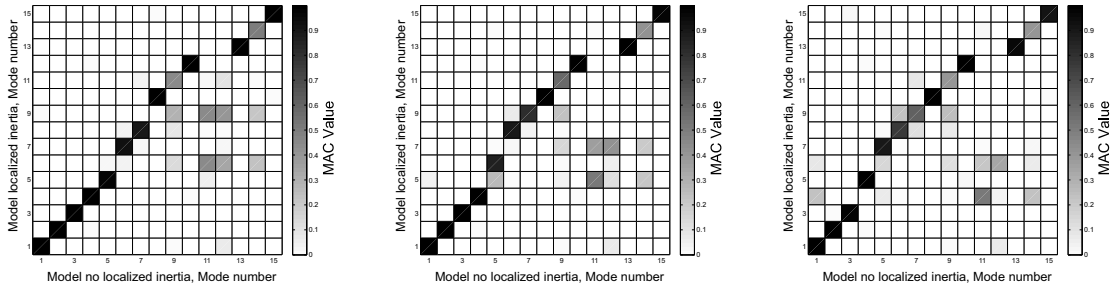

(a) 1% and 5% non-structural masses (b) 5% and 10% non-structural masses (c) 10% and 20% non-structural masses

Figure 13: MAC values between the initial model and the model with non-structural mass; industrial building Case C CW approach.

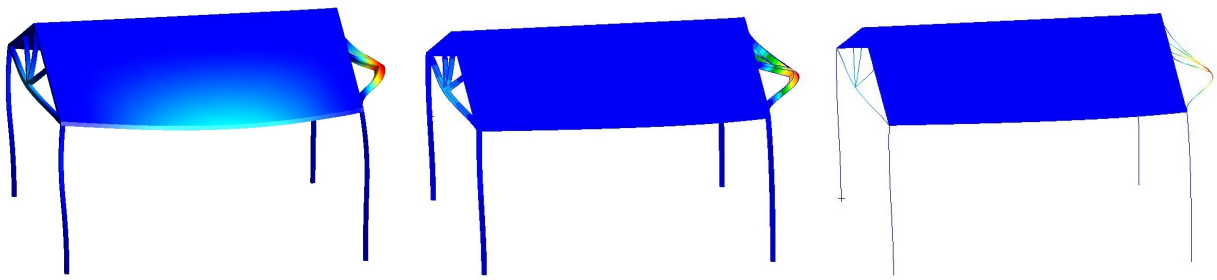

(a) CW Model (b) Solid Model (c) 1D&2D Model

Figure 14: 4^{th} modal shape of the industrial building, 5% and 10% non-structural masses.

The third case considers a combination of two non-structural masses on the roof truss. Their presence deeply influences the local behaviour of the structure, causing the change in its modal shapes. For example, the 4^{th} modal shape is reported in Fig. 14. This alteration can be clearly observed also in the MAC values reported in Fig. 13.

Subsequently, the effect of a distributed mass acting on the whole roof is investigated (e.g in the case of a heavy snowfall). Regulations prescribe to take into account the loads originating from this situation as a design parameter. Thus, a load of 1.5 kN/m^2 was considered, as stated in [35]. The natural frequencies are reported in Table 7, whereas the modal shapes are shown in Fig. 15. Moreover, the MAC matrix for this case is shown in Fig. 16. It is clear that the presence of additional mass on the roof causes a global decrease of

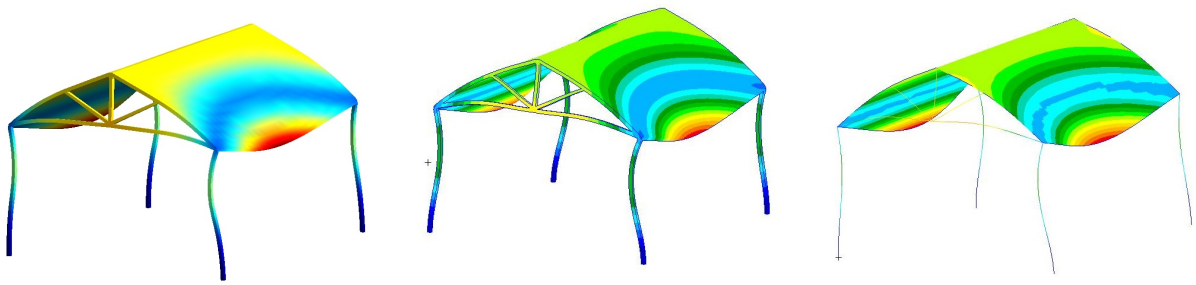

(a) CW Model (b) Solid Model (c) 1D&2D Model

Figure 15: 6^{th} modal shape of the industrial building in the case of distributed mass.

Distributed mass			
DOFs	CW model (6399)	NAS1D&2D (2836)	NAS3D (143121)
Mode 1^b	0.56	0.47	0.48
Mode 2^t	0.97	0.80	0.83
Mode 3^r	4.21	4.04	4.12
Mode 4^c	9.50	8.96	9.18
Mode 5^r	10.93	10.23	10.43

b: bending mode; t: torsional mode.
c: coupled roof and truss mode; r: local roof mode.

Table 7: Natural frequencies (Hz) of the industrial building, distributed non-structural mass.

the frequencies. Moreover, from the observation of the MAC matrix in Fig. 16 it can be highlighted the swap

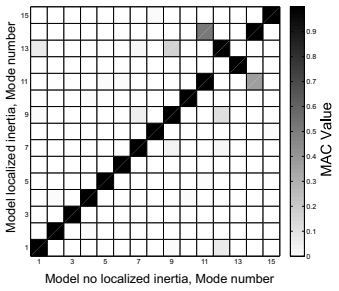

(a) distributed mass

Figure 16: MAC values between the initial model and the model with distributed non-structural mass, industrial building, CW approach.

between the 12^{th} and the 13^{th} modal shapes. On the other hand, the figure shows a good correspondance between the remaining modal shapes of the initial model and and those of the distributed mass model.

5.3 Three-floor building

In this section, the three-floor building analyzed in [19] is considered. The natural frequencies of the initial model are reported in Table 8. Free vibration analysis is performed for three different cases: the first case takes into account the mass of a garden on the rooftop whereas the second and the third case the mass of a heavy piece of furniture on the floor. In Case A, a distributed mass of 8400kg is applied on the tip cross section, whereas in Cases B and C four 250kg masses are located on four different points of the first and second floor, respectively. The initial model and the three cases are shown in Fig.17, whereas the coordinates of the four masses for Cases B and C are reported in Table 9. Natural frequencies obtained using a coarse and a finer CW model are reported in Tables 10, 11 and 12, respectively. Moreover, the results obtained by means of MSC Nastran are given for comparison. Fig.18 shows the difference between the initial model and those with non-structural mass, which is evaluated through MAC analysis.

DOFs	CW (coarse) (11592)	CW (finer) (19548)	NAS3D (218286)
Mode 1	9.87^b	9.62^b	9.51^b
Mode 2	10.29^b	10.08^b	10.04^b
Mode 3	13.99^t	13.69^t	13.63^t
Mode 4	27.74^f	15.97^f	16.18^f
Mode 5	28.23^f	16.41^f	16.61^f
Mode 6	28.40^b	16.47^f	24.78^b
Mode 7	31.11^b	26.22^b	25.04^b
Mode 8	31.49^f	26.58^b	28.48^f
Mode 9	31.51^f	32.59^b	28.94^f

b: bending mode ; t: torsional mode; f: floor mode.

Table 8: Natural frequencies (Hz) of the three-floor building.

Given the distribution of the masses, it is clear that a finer discretization of the floors should be adopted. The results show that the coarse CW model is capable to detect with a good degree of accuracy the global

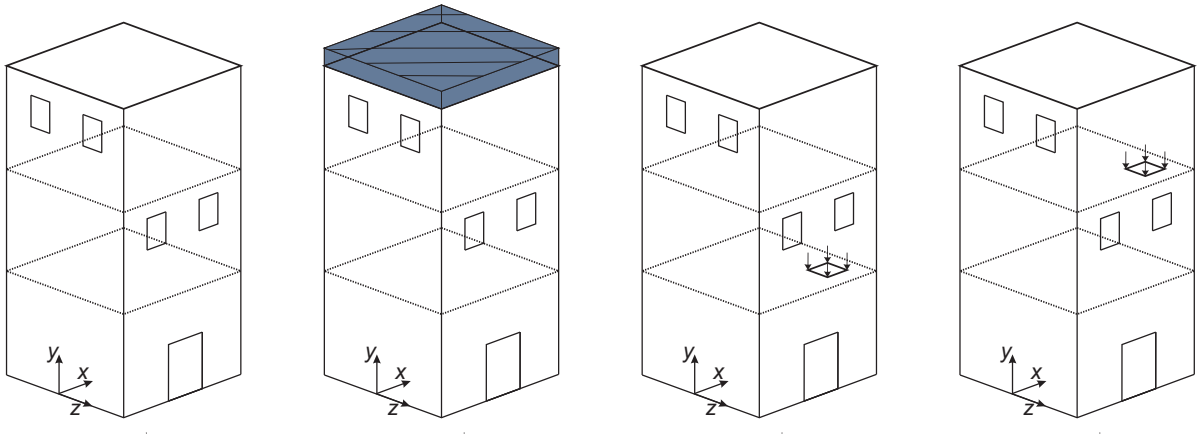

(a) Initial Model (b) Case A (c) Case B (d) Case C

Figure 17: Three-floor building and non-structural mass localization for the three different cases.

	X[m]	Z[m]
Point 1	3.0	1.44
Point 2	3.0	2.0
Point 3	3.56	1.44
Point 4	3.56	2.0

Table 9: Location of non-structural masses, cases B and C.

Case A			
DOFs	CW (coarse) (11592)	CW (finer) (19548)	NAS3D (218286)
Mode 1	9.10^b	8.88^b	8.77^b
Mode 2	9.44^b	9.26^b	9.21^b
Mode 3	13.30^t	11.01^f	11.31^f
Mode 4	19.41^f	13.04^t	12.98^t
Mode 5	26.08^b	16.41^f	16.59^f
Mode 6	26.49^b	16.46^f	16.79^f
Mode 7	31.02^f	23.73^f	22.51^f
Mode 8	31.46^f	23.79^f	22.57^f
Mode 9	37.44^w	24.98^b	24.01^b

b: bending mode ; t: torsional mode;
f: floor mode; w: wall mode.

Table 10: Natural frequencies (Hz) of the three-floor building undergoing non-structural mass, Case A.

modes which involve the whole structure. However, this model yields to poor results when the local modes of the floors are considered. On the other hand, the finer CW model is capable to detect the effects due to non-structural masses with a higher degree of accuracy. It is evident that the results obtained with the CW finer mesh are in good accordance with those provided by the Nastran 3D model. Moreover, these results are obtained with a dramatic reduction in computational efforts, as reported in row 3 of Tables 10, 11 and 12.

Case B			
DOFs	CW (coarse) (11592)	CW (finer) (19548)	NAS3D (218286)
Mode 1	9.85^b	9.61^b	9.48^b
Mode 2	10.27^b	10.06^b	10.02^b
Mode 3	13.98^t	13.69^t	13.63^t
Mode 4	26.87^f	14.02^f	14.15^f
Mode 5	27.43^b	15.97^f	16.19^f
Mode 6	27.94^b	16.42^f	16.69^f
Mode 7	28.49^f	25.95^b	24.56^b
Mode 8	31.12^f	26.33^b	24.84^b
Mode 9	37.50^w	29.02^l	26.53^l

b: bending mode ; t: torsional mode;
f: floor mode; w: wall mode.

Table 11: Natural frequencies (Hz) of the three-floor building undergoing non-structural mass, Case B

Case C			
DOFs	CW (coarse) (11592)	CW (finer) (19548)	NAS3D (218286)
Mode 1	9.80^b	9.56^b	9.47^b
Mode 2	10.22^b	10.02^b	9.97^b
Mode 3	13.97^t	13.68^t	13.62^t
Mode 4	26.64^f	14.00^f	14.12^f
Mode 5	27.72^b	15.97^f	16.20^f
Mode 6	28.20^b	16.46^f	16.72^f
Mode 7	28.52^f	26.16^b	24.57^b
Mode 8	31.49^f	26.48^b	24.89^f
Mode 9	37.49^w	29.23^l	27.16^l

b: bending mode ; t: torsional mode;
f: floor mode; w: wall mode.

Table 12: Natural frequencies (Hz) of the three-floor building undergoing non-structural mass, Case C.

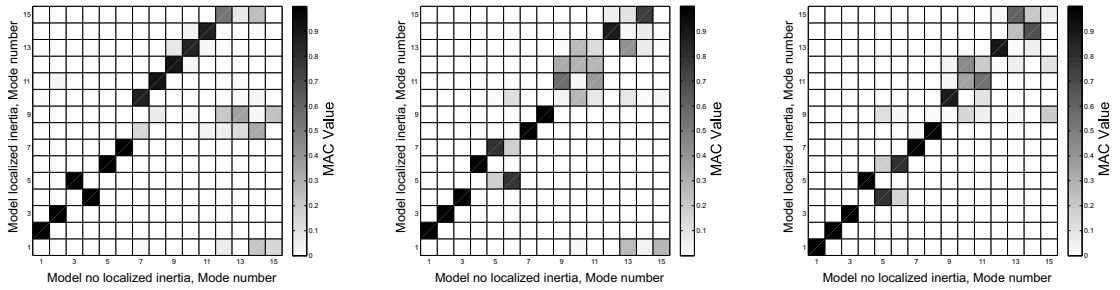

(a) Case A (b) Case B (c) Case C

Figure 18: MAC values between the initial model and the model with non-structural mass of the three-floor building, finer CW mesh.

6 Conclusions

The influence of non-structural masses on the free vibrations of typical civil engineering structures has been investigated in this paper. The presence of these elements causes bending/torsion couplings and local phenomena which involve large distortions of the cross section. Thus, classical beam theories provide unreliable

results and the analyses performed required higher-order models. The proposed theories have been developed in the framework of the Carrera Unified Formulation (CUF), adopting the Component-Wise (CW) approach. This approach allows us to model each part of a multi-component structure as a refined 1D beam element. As demonstrated in previous works, localized boundary conditions can be addressed with no need of ad hoc mathematical procedures. The CW models have demonstrated the capabilities of this formulation in the investigation of localized inertia effects. Moreover, the comparison between the results obtained by means of the CW approach and those obtained using the MSC Nastran code has shown a good accordance between the two models. Thus, the high level of accuracy and the lower computational cost of the CUF models are demonstrated.

References

[1] J.M. Deb Nath. Free vibration, stability and non-classical modes of cooling tower shells. *Journal of Sound and Vibration*, 33(1):79 – 101, 1974. doi : 10.1016/S0022-460X(74)80075-1.

[2] T.Y. Yang and R.K. Kapania. Shell elements for cooling tower analysis. *Journal of Engineering Mechanics*, 109(5):1270–1289, 1983.

[3] Q. Zhang, T. Chang, and C. Chang. Finite-Element model updating for the Kap Shui Mun cable-stayed Bridge. *Journal of Bridge Engineering*, 6(4):285–293, 2001. doi : 10.1061/(ASCE)1084-0702(2001)6:4(285).

[4] W. Ren, G. Blandford, and I. Harik. Roebling suspension Bridge. I: Finite-element model and free vibration response. *Journal of Bridge Engineering*, 9(2):110–118, 2004. doi : 10.1061/(ASCE)1084-0702(2004)9:2(110).

[5] J. Lee, M. Bang, and J.Y. Kim. An analytical model for high-rise wall-frame structures with outriggers. *The Structural Design of Tall and Special Buildings*, 17(4):839–851, 2008. doi: 10.1002/tal.406.

[6] J. S. Kuang and S. C. Ng. Lateral shear-St. Venant torsion coupled vibration of asymmetric-plan frame structures. *Structural Design of Tall Special Buildings*, 18:647–656, 2009. doi: 10.1002/tal.456.

[7] X. Li, J. Cai, and S. Qiang. Train running safety and riding comfort analysis of the schemed Nanjing Yangtze-River Bridge on Beijing-Shanghai high-speed railway. *Process in Safety Science and Technology Part A*, 3:346–352, 2002.

[8] A. Bayraktar, A. Sahin, D.M. Oezcan, and F. Yildirim. Numerical damage assessment of Haghia Sophia Bell Tower by Nonlinear FE Modeling. *Applied Mathematical Modeling*, 34:92–121, 2010. doi: 10.1016/j.apm.2009.03.033.

[9] P. Riva, F. Perotti, E. Guidoboni, and E. Boschi. Seismic analysis of the Asinelli Tower and earthquakes in Bologna. *Soil Dynamics and Earthquake Engineering*, 17(7):525–550, 1998. doi: 10.1016/S0267-7261(98)00009-8.

[10] C. Lang. Free vibration and earthquake behavior of solar power plant chimneys. *ECCOMAS Thematic Conference - COMPDYN 2011: 3rd International Conference on Computational Methods in Structural Dynamics and Earthquake Engineering: An IACM Special Interest Conference, Programme*, 2011.

[11] H.B. Xu, C.W. Zhang, H. Li, P. Tan, J.P. Ou, and F.L. Zhou. Active mass driver control system for suppressing wind-induced vibration of the Canton Tower. *Smart Structures and Systems*, 13(2):281–303, 2014. doi : 10.12989/sss.2014.13.2.281.

[12] S. Ivorra and F. J. Pallarés. Dynamic investigations on a masonry bell tower. *Engineering Structures*, 28(5):660–667, 2006. doi: 10.1016/j.engstruct.2005.09.019.

[13] E. Carrera. Theories and finite elements for multilayered, anisotropic, composite plates and shells. *Archives of Computational Methods in Engineering*, 9(2):87–140, 2002. doi: 10.1007/BF02736649.

[14] E. Carrera. Theories and finite elements for multilayered plates and shells: a unified compact formulation with numerical assessment and benchmarking. *Archives of Computational Methods in Engineering*, 10(3):216–296, 2003. doi: 10.1007/BF02736224.

[15] E. Carrera and G. Giunta. Refined beam theories based on a unified formulation. *International Journal of Applied Mechanics*, 2(1):117–143, 2010. doi: 10.1142/S1758825110000500.

[16] E. Carrera and M. Petrolo. On the effectiveness of higher-order terms in refined beam theories. *Journal of Applied Mechanics*, 78, 2011. doi: 10.1115/1.4002207.

[17] E. Carrera, M. Maiaru, and M. Petrolo. Component-wise analysis of laminated anisotropic composites. *International Journal of Solids and Structures*, 49:1839–1851, 2012. doi: 10.1016/j.ijsolstr.2012.03.025.

[18] E. Carrera, A. Pagani, and M. Petrolo. Classical, refined and component-wise analysis of reinforced-shell wing structures. *AIAA Journal*, 51(5):1255–1267, 213. doi: 10.2514/1.J052331.

[19] E. Carrera and A. Pagani. Free vibration analysis of civil engineering structures by component-wise methods. *Journal of Sound and Vibration*, 333:4597–4620, 2014. doi: 10.1016/j.jsv.2014.04.063.

[20] E. Carrera, A. Pagani, and M. Petrolo. Refined 1D finite elements for the analysis of secondary, primary and complete civil engineering structures. *Journal of Structural Engineering*, 2014. doi: 10.1061/(ASCE)ST.1943-541X.0001076.

[21] E. Carrera, A. Pagani, and Zangallo F. Thin-walled beams subjected to load factors and non-structural masses. *International Journal of Mechanical Sciences*, 81:109–119, 2014. doi: 10.1016/j.ijmecsci.2014.02.015.

[22] A. Pagani, F. Zangallo, and E. Carrera. Influence of non-structural localized inertia on free vibration response of thin-walled structures by variable kinematic beam formulations. *Shock and Vibration*, 2014:141982/1–16, 2014. doi: 10.1155/2014/141982.

[23] E. Carrera and A. Pagani. Accurate response of wing structures to free-vibration, load factors, and nonstructural masses. *AIAA Journal*, 54(1):227–241, 2016. doi: 10.2514/1.J054164.

[24] A. Reggio and M. De Angelis. Combined primary-secondary system approach to the design of an equipment isolation system with high-damping rubber bearings. *Journal of Sound and Vibration*, 333(9):2386 – 2403, 2014. doi: 10.1016/j.jsv.2013.12.006.

[25] A.B. Aldeka, A.H.C. Chan, and S. Dirar. Response of non-structural components mounted on irregular rc buildings: Comparison between fe and ec8 predictions. *Earthquake and Structures*, 6(4):351–373, 2014. doi: 10.12989/eas.2014.6.4.351.

[26] M. E. Rodriguez, J. I. Restrepo, and A. J. Carr. Earthquake-induced floor horizontal accelerations in buildings. *Earthquake Engineering & Structural Dynamics*, 31(3):693–718, 2002. doi: 10.1002/eqe.149.

[27] R. K. L. Su, A. M. Chandler, M. N. Sheikh, and N. T. K. Lam. Influence of non-structural components on lateral stiffness of tall buildings. *The Structural Design of Tall and Special Buildings*, 14(2):143–164, 2005. doi: 10.1002/tal.266.

[28] E. Carrera, A. Pagani, M. Petrolo, and E. Zappino. Recent developments on refined theories for beams with applications. *Mechanical Engineering Reviews*, 2(2), In press. ISSN 2187-9753.

[29] E. Carrera, M. Petrolo, and P. Nali. Unified formulation applied to free vibrations finite element analysis of beams with arbitrary section. *Shock and Vibration*, 18(3):485–502, 2011. doi: 10.3233/SAV-2010-0528.

[30] A. Pagani, M. Boscolo, J. R. Banerjee, and E. Carrera. Exact dynamic stiffness elements based on one-dimensional higher-order theories for free vibration analysis of solid and thin-walled structures. *Journal of Sound and Vibration*, 332(23):6104–6127, 2013. doi: 10.1016/j.jsv.2013.06.023.

[31] E. Carrera, G. Giunta, and M. Petrolo. *Beam Structures Classical and Advanced Theories*. John Wiley & Sons, Ltd, The Atrium, Southern Gate, Chichester, West Sussex, PO19 8SQ, United Kingdom, 2011.

[32] E. Carrera, M. Cinefra, M. Petrolo, and E. Zappino. *Finite Element Analysis of Structures through Unified Formulation*. John Wiley & Sons Ltd, 2014.

[33] E. Carrera and M. Petrolo. Refined beam elements with only displacement variables and plate/shell capabilities. *Meccanica*, 47(3), 2012. doi: 10.1007/s11012-011-9466-5.

[34] E. Carrera, A. Pagani, and M. Petrolo. Use of lagrange multipliers to combine 1D variable kinematic finite elements. *Computers and Structures*, 129:194–206, 2013. doi: 10.1016/j.compstruc.2013.07.005.

[35] P. Formichi. EN 1991 Eurocode 1: Actions on structures Part 1-3 General actions Snow Loads, 2008. url : http://eurocodes.jrc.ec.europa.eu/doc/WS2008/EN1991_3_Formichi.pdf.